arXiv:astro-ph/0703204v1 9 Mar 2007

J. Astrophys. Astr. (0000) **00**, 000–000

GMRT and VLA observations at 49cm and 20cm of the HII region near $l = 24^\circ.8$, $b = 0.^\circ1$

N. G. Kantharia[1], W. M. Goss[2], D. Anish Roshi[3],
Niruj R. Mohan[4], Francois Viallefond[5]
[1]*National Centre for Radio Astrophysics, TIFR, Post Bag 3, Ganeshkhind, Pune-411007, India*
[2]*National Radio Astronomy Observatory, P.O.Box 0, Socorro, NM 87801, USA*
[3] *Raman Research Institute, Sadashivnagar, Bangalore-560080, India*
[4] *Sterrewacht, Leiden, The Netherlands*
[5]*Observatoire de Paris, Paris, France*

Received/Accepted 8 March 2007

Abstract.

We report multifrequency radio continuum and hydrogen radio recombination line observations of HII regions near $l = 24^\circ.8$ $b = 0^\circ.1$ using the Giant Metrewave Radio Telescope (GMRT) at 1.28 GHz (n=172), 0.61 GHz (n=220) and the Very Large Array (VLA) at 1.42 GHz (n=166). The region consists of a large number of resolved HII regions and a few compact HII regions as seen in our continuum maps, many of which have associated infrared (IR) point sources. The largest HII region at $l = 24^\circ.83$ and $b = 0^\circ.1$ is a few arcmins in size and has a shell-type morphology. It is a massive HII region enclosing $\sim 550\ M_\odot$ with a linear size of 7 pc and an rms electron density of ~ 110 cm^{-3} at a kinematic distance of 6 kpc. The required ionization can be provided by a single star of spectral type O5.5.

We also report detection of hydrogen recombination lines from the HII region at $l = 24.83^\circ$ and $b = 0.1^\circ$ at all observed frequencies near $V_{lsr} = 100$ kms^{-1}. We model the observed integrated line flux density as arising in the diffuse HII region and find that the best fitting model has an electron density comparable to that derived from the continuum. We also report detection of hydrogen recombination lines from two other HII regions in the field.

Key words: Interstellar medium: Radio recombination lines: HII regions: Envelopes.

1. Introduction

Since the discovery of radio recombination lines (RRLs) (Dravskikh & Dravskikh 1964 ; Sorochenko & Borozich 1964 ; Palmer et al. 1967) these have been widely

used as diagnostics of ionized media in the Galaxy. Theoretical studies of line formation have shown that the width of RRLs depends sensitively on the principal quantum number ($\Delta\nu \propto n^{4.4}$; $\Delta\nu$ in Hz) and is also proportional to the electron density (Shaver 1975). Thus low-frequency ($<$ a few GHz) RRLs from dense ionized regions ($>$ a few times 10^2 cm^{-3}) will be broadened, resulting in the reduction of the peak line intensity. This reduction in peak intensity makes it difficult to detect RRLs at low frequencies from high density gas. On the other hand, low frequency RRLs from low density ionized regions are not affected by this limitation. Hence these RRLs form an ideal probe to study lower density regions such as photodissociation regions, diffuse, extended HII regions (e.g. Lockman 1989 , Lockman et al. 1996), envelopes of HII regions and the extended low density warm ionized medium (ELDWIM) (Roshi & Anantharamaiah 2001 , Anantharamaiah 1985 , Heiles et al. 1996). Typically such regions have densities ≤ 100 cm^{-3} and emission measures $\leq 10^5$ pc cm^{-6}.

In this paper, we present Giant Metrewave Radio Telescope (GMRT) and Very Large Array (VLA) observations of the HII region complex near $l = 24^\circ.8$ and $b = 0^\circ.1$ in RRLs and radio continuum at frequencies of 0.61, 1.28 and 1.42 GHz. This region consists of HII regions in various evolutionary stages, ranging from protostellar stage showing bipolar outflows detected in CO (Furuya et al. 2002) to the diffuse, extended HII region like G24.83+0.10. The primary objective of these observations were to image and determine the physical properties of the diffuse HII region from which low frequency hydrogen and carbon RRLs near 327 MHz have been observed (Anantharamaiah 1985). The details of the observations are given in Section 2. The radio continuum morphology and physical properties of the diffuse HII regions derived from the continuum are described in Section 3 . In Section 4, we present the RRL data. We end with a summary of the results. A near kinematic distance of 6 kpc was determined for G24.83+0.10 and is used in this paper.

2. Observations

Table 1 gives the details of the observation. The 0.61 and 1.28 GHz observations were carried out with the GMRT and the 1.42 GHz observations were carried out with the VLA.

2.1 *GMRT observations: 0.61 and 1.28 GHz*

The GMRT (Swarup et al. 1991 & Ananthakrishnan & Rao 2002) consists of 30 45-m diameter dishes spread over a 25 km region and operating in five frequency bands. For our 1.28 GHz observations, we selected a 2 MHz bandwidth which includes both the H172α and the C172α lines. We followed an observing sequence of 20 min on-source followed by 6 min on the phase calibrator. The bandpass calibrator was observed thrice during the run for 30 min each. After editing corrupted data, we were left with 23 antennas on 13 April 2002 and 17 antennas on 14 April 2002, which were used in the subsequent analysis.

Table 1. Observation details

Parameter	0.610 GHz	1.28 GHz	1.42 GHz
Telescope	GMRT	GMRT	VLA (C, DnC)
Field of view	$\sim 44'$	$\sim 25'$	$\sim 40'$
Phase centre			
α_{2000}	$18^h36^m11^s$	same	same
δ_{2000}	$-07^\circ10'40''$	same	same
Date of	17/1/2003	13/4/2002	5/10/2002,
Observation		14/4/2002	13/12/2002,
			20/1/2003
Transitions	H220α	H172α	H166α
	C220α	C172α	C166α
Rest Freq			
Hydrogen (GHz)	0.613405	1.28117	1.42473
Carbon (GHz)	0.613711	1.28181	1.42544
Phase cal	1822-096	1822-096	1831-126
Flux cal	3C286,3C48	3C286,3C48	1923+210
Bandpass cal	1822-096	3C286,3C48	3C48
Bandwidth (km s^{-1})	480	480	330
Channel width (km s^{-1})	3.8	3.7	2.6
Resolution			
continuum	$14'' \times 7''$	$8'' \times 6''$	$35'' \times 25''$
PA	-24°	38°	40°
line	$22'' \times 22''$	$23'' \times 12''$	$35'' \times 25''$
PA	-57°	42°	40°
RMS noise			
contm (mJy/beam)	2	2	4
line (mJy/beam)	3	2	3

At 0.61 GHz, we selected a bandwidth of 1 MHz which includes both the hydrogen ($H220\alpha$) and carbon ($C220\alpha$) lines. The observing procedure was similar to that used at 1.28 GHz.

The GMRT data were converted to FITS format and imported into the NRAO AIPS package for further analysis. Single channel data on the bandpass calibrators were first examined, edited and gain calibrated. Bandpass solutions were then generated on these calibrators, which were applied to the data on all objects before averaging the line free channels to generate the continuum database. A first order spectral baseline was removed from the calibrated uv line data using the task UVLIN. The final continuum and line images were generated using IMAGR. The estimated flux density scale has errors $\leq 20\%$.

At the time of our observations, noise switching to measure the system temperature was not available. We estimated the difference in system temperature between

the primary calibrator and the target source positions using the 0.408 GHz continuum map (Haslam 1982) and assuming a spectral index for the galactic background emission of -2.7. These correction factors were then applied to the data.

2.2 *VLA observations: 1.42 GHz*

The VLA observations were conducted with a bandwidth of 1.5 MHz which contained the observing frequencies for both the H166α and the C166α lines toward G24.83+0.10. Observing details are listed in Table 1. Data were obtained in the C and DnC configurations. The observations on the target source were interspersed with 5 min runs on the phase calibrator. The bandpass calibrator was observed at the beginning and end of the run for about 10 min. Data from all the three short runs were combined to obtain the final dataset. These data were online Hanning smoothed. The VLA data were analysed using standard tasks in AIPS. The continuum image was made by using the central 75% of the total number of channels. Gain and bandpass calibration were then carried out and applied to continuum and line data. The continuum emission was removed from the line uv data using UVLSF in AIPS. This data was then used to generate a cube using IMAGR. For further analysis, moment maps were also generated.

3. The Continuum Emission

Fig. 1 and 2 show the continuum images. The 1.28 (Fig. 1a) and 0.61 (Fig. 1b, Fig. 2b) GHz continuum images were obtained after applying a UV taper of 30 kλ. At 1.28 GHz, the largest angular scale to which the GMRT is sensitive is $\sim 7'$, thus the images are likely missing flux density for the large scale components. We, therefore, use the 0.61 and 1.42 GHz data to derive the spectral index listed in Table 2. The compact sources are marked in the 1.28 GHz image (see Fig 1a). Resolved sources within the field of view of the observations are marked in the 1.42 GHz image shown in Fig. 2a. Table 2 lists the estimated flux densities of these diffuse sources after correcting for the primary beam attenuation. IRAS point sources are marked by crosses in Fig. 2a.

Infrared sources are associated with most of the diffuse regions shown in the Fig 2a. To ascertain that these are not chance superpositions, we examined the 60μm flux density of these sources as given in the IRAS PSC and these are plotted in Fig. 2. Codella et al. (1994) have shown that IRAS PSC sources which have $S_{60\mu}m > 100$Jy have more than 80% probability of being associated with HII regions and that for sources with $S_{60\mu}$m> 300Jy, chance superpositions are expected to be very rare. The $S_{60\mu}$m for all the sources are plotted in Fig. 2b. As seen here, almost all the sources lying on the diffuse sources have a flux density > 100 Jy at 60μm and most of them have flux densities > 300 Jy totally ruling out chance superpositions. The IRAS sources seen in rest of the field have lower flux densities at 60μm and hence are unlikely to be associated with HII regions.

In rest of this section, we discuss the continuum emission from these diffuse

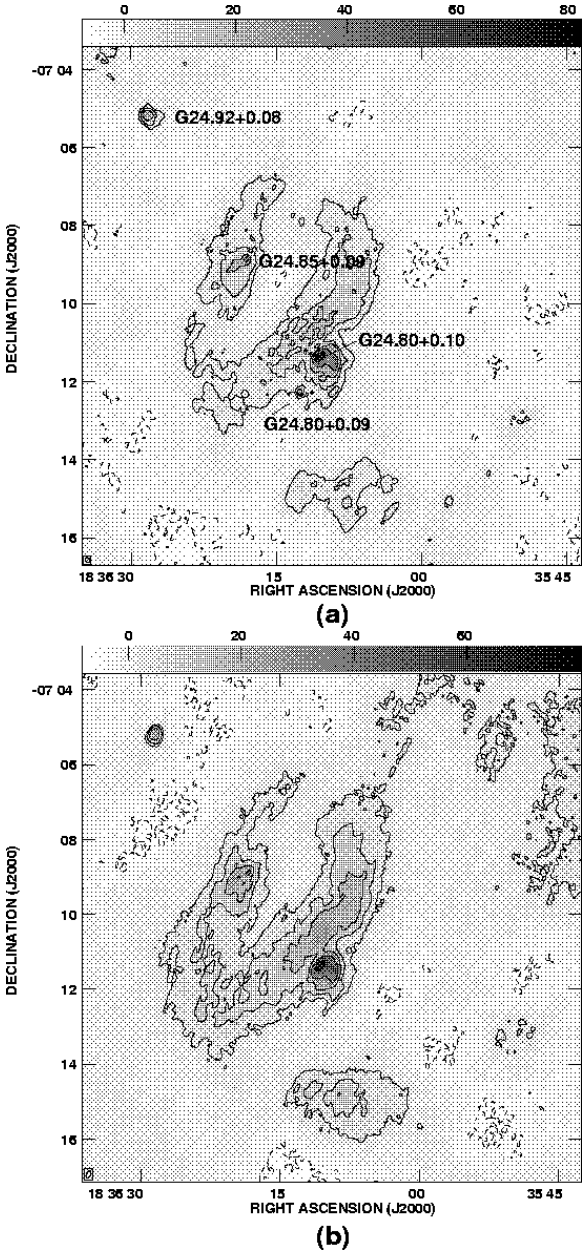

Figure 1. (a) GMRT 1.28 GHz continuum image of the region near $l = 24°.8$, $b = 0°.1$ with an angular resolution of $8.4'' \times 6.3''$, PA $= 38°$. The RMS noise in the image is 1.5 mJy/beam. The grey scale ranges from -7 mJy/beam to 82 mJy/beam. The contour levels are -7.5, -3.75, 3.75, 7.5, 15, 30, 60, 120, 240, 480 mJy/beam. The compact sources detected in the field are labelled. (b) GMRT 0.61 GHz continuum image of the region near $l = 24°.8$, $b = 0°.1$. The angular resolution of the image is $13.8'' \times 6.7''$, PA $= -24°$ and the RMS noise is 1.6 mJy/beam. The grey scale ranges from -8 mJy/beam to 80 mJy/beam. The contour levels are -8, -4, 4, 8, 16, 32, 64, 128, 256, 512 mJy/beam.

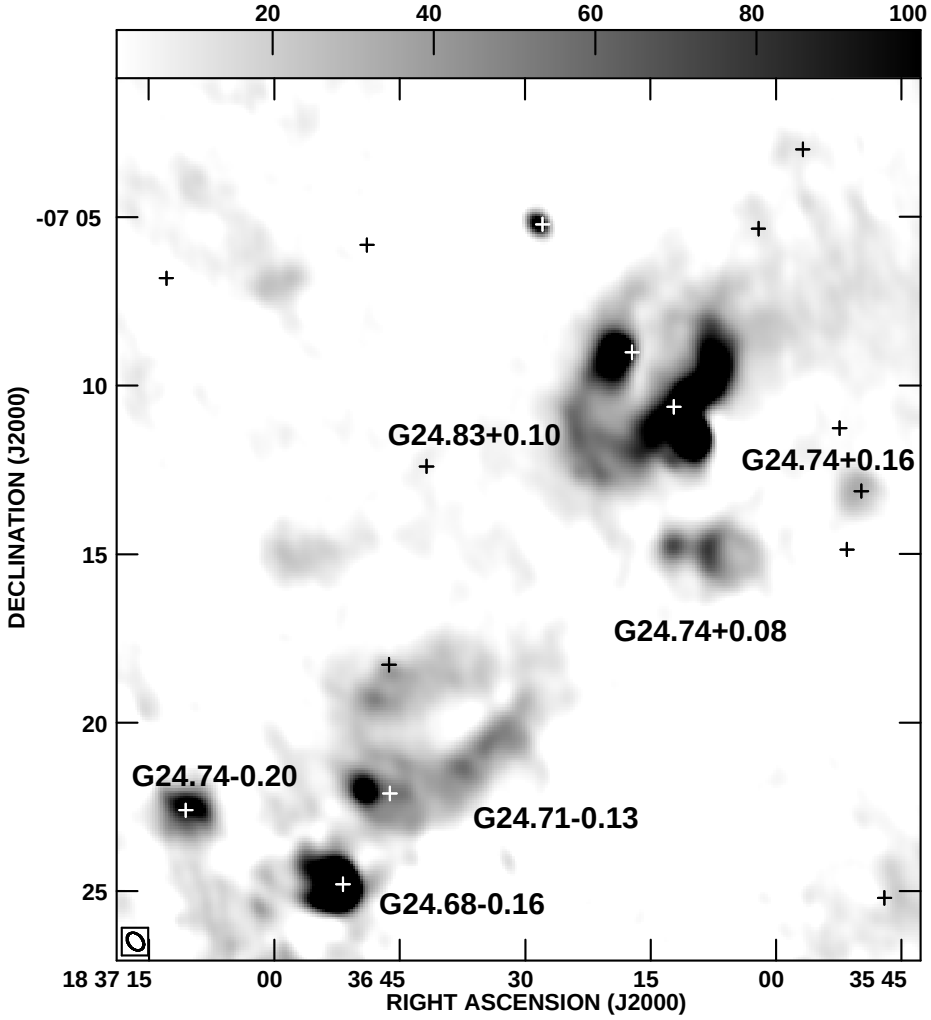

Figure 2. (a) VLA radio continuum image at 1.42 GHz of the field near $l = 24^{\circ}.8, b = 0^{\circ}.1$. The image has been smoothed to a resolution of $35'' \times 25''$, PA $= 40^{\circ}$. The grey scale is plotted from 1 mJy/beam to 100 mJy/beam. The image has been corrected for primary beam attenuation. The diffuse HII regions (angular size $\geq 1'$) in the field are labelled. Crosses mark positions of IRAS point sources in the region obtained from the IRAS PSC.

sources alongwith the associated IRAS point sources. The radio continuum peaks in the diffuse regions are likely indicating the positions of the exciting stars.

G24.83+0.10 : The brightest diffuse source in the field of view is G24.83+0.10. The integrated flux density of this source at 1.42 GHz is 7.7 Jy. Higher resolution images of this source are shown in Fig 1. The diffuse source has a shell-like morphology with multiple radio peaks. The size of the shell is about 7 pc. The spectral

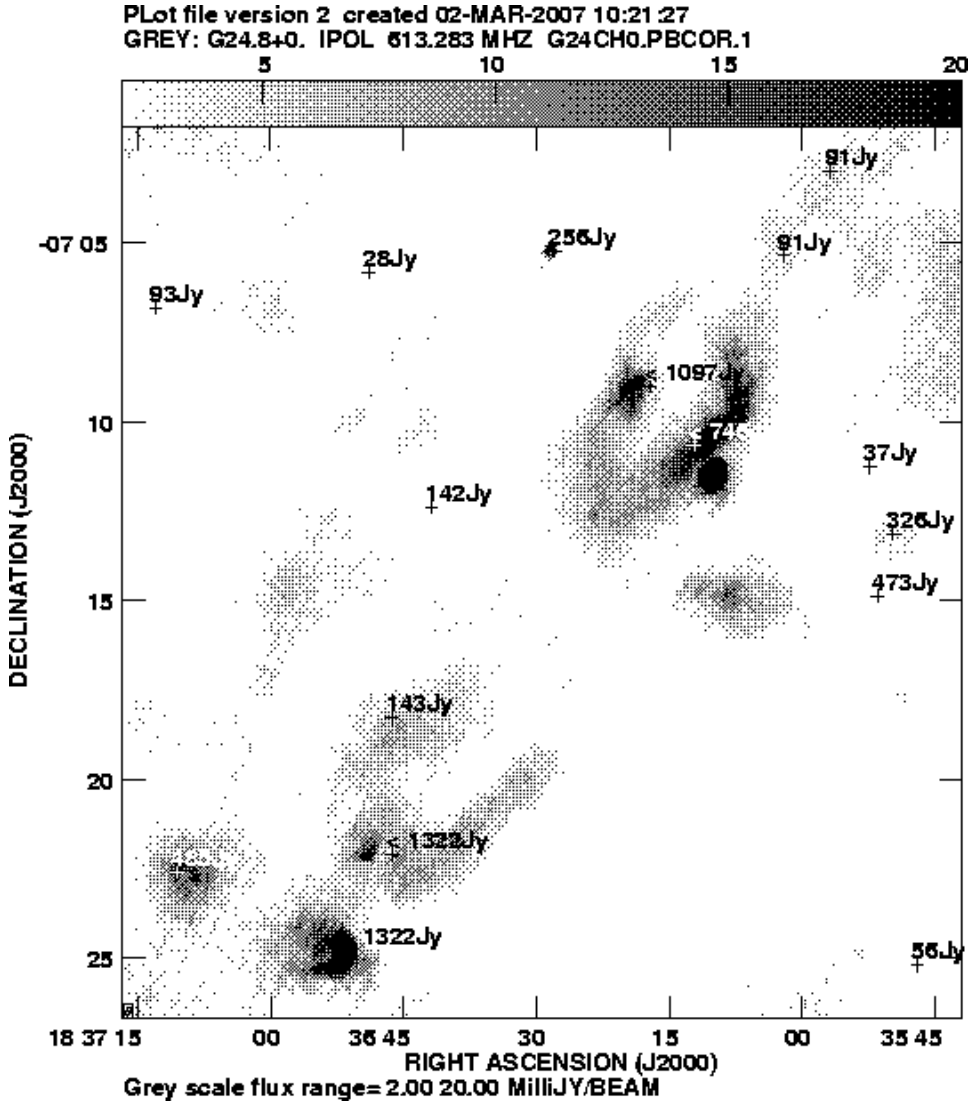

Figure 2. (b) GMRT image of the same field as in (a) at 0.61 GHz. The image has an angular resolution of $14'' \times 7''$, PA $= -24°$. The grey scale is plotted from 2 mJy/beam to 20 mJy/beam. The image has been corrected for primary beam attenuation. The crosses mark the positions of sources from the IRAS PSC. The strength of these sources at 60μm are marked.

index of this HII region is consistent with optically thin free free emission. Two IRAS point sources are coincident with this object as shown in Fig. 2. The IR emission arises from the thermal dust located within the OB associations heated by the stars (Conti & Crowther 2004). At higher angular resolutions and frequencies, several compact/ultracompact HII regions are detected in G24.80+0.09. The

Table 2. Continuum flux densities and derived spectral indices using 0.61 and 1.42 GHz data of the diffuse HII regions marked in Fig. 2. Since some of the regions lie outside the 1.28 GHz primary beam, no flux density at this frequency is available.

Source	ν GHz	Flux density[1] Jy	$\alpha_{1.42GHz}^{0.61GHz}$	IRAS Pt src
G24.83+0.10	0.61	8.4	$-0.1^{-0.2}_{+0.3}$	IRAS 18335-0713A
	1.28	5.3		IRAS 18335-0711
	1.42	7.7		
	4.87[2]	7.1		
G24.74+0.08	0.61	1.29	$-0.6^{-0.2}_{+0.3}$	-
	1.28	0.65		
	1.42	0.80		
G24.74+0.16	0.61	0.21	$-0.4^{-0.2}_{+0.3}$	IRAS 18331-0715
	1.42	0.15		
G24.68−0.16	0.61	2.6	$-0.15^{-0.2}_{+0.25}$	IRAS 18341-0727
	1.42	2.3		
G24.71−0.13	0.61	3.9	$-0.3^{-0.2}_{+0.25}$	IRAS 18340-0724
	1.42	3.0		
G24.74−0.2	0.61	1.4	$-0.85^{-0.15}_{+0.2}$	IRAS 18344-0725
	1.42	0.68		

[1] The error in flux density at 0.61 GHz and 1.28 GHz is $\leq 20\%$. The error bars on the spectral index are estimated using a conservative 20% error on the 0.61 GHz data points.
[2] Data from Downes et al. (1980).

ultracompact HII regions in G24.8+0.09 have been extensively studied at higher frequencies with high angular resolution (for example, Furuya et al. 2002). These HII regions are found to be in an earlier stage of evolution (Furuya et al. 2002). The UV photons from the stars exciting the UC HII regions might be absorbed by dust resulting in photon-bound UC HII regions. The other peak in the W arc, ie G24.80+0.10 appears to be a cometary type HII region with a tail extending to the N along the diffuse arc. The IRAS point source IRAS 18335-0713A is located in the W arc of G24.83+0.10, close to G24.80+0.10 and has a flux density of 746 Jy at 60 μm. G24.80+0.10 (which appears as a single radio peak in the VLA 20 cm

Table 3. The physical parameters derived from the measured continuum flux density of the source at 1.42 GHz are listed below. We assumed an electron temperature of 7000 K for the HII region and a spherical geometry. The exciting star is tabulated from Panagia (1973). All the regions are taken to be at a kinematic distance of 6 kpc.

Source	$< \mathbf{N_e} >$ cm^{-3}	**d** pc	$< \mathbf{EM} >$ 10^4 pccm^{-6}	**Mass** $M_\odot$	$\mathbf{N_{Lyc}}$ 10^{48} sec^{-1}	Exc star
G24.83+0.10	110	7	9.0	550	23	O5.5
G24.74+0.08	90	4	3.5	70	2	O8
G24.74+0.16	75	3	1.5	15	0.4	B0
G24.68-0.16	160	4	9.5	120	7	O6.5
G24.71-0.13	70	7	3.5	340	9	O6
G24.74-0.20	160	3	6.5	35	2	O8

image (see Fig 2)) is resolved into a double peaked structure in the higher resolution GMRT images at 20 cm and 49 cm. Another compact HII region G24.85+0.09 (see Fig 1a) is located in the E arc of this diffuse HII region. This region also seems to display a cometary structure. The IRAS point source IRAS 18335-0711 with a flux density of 1097 Jy at 60μm is associated with this region.

We have used the VLA data at 1.42 GHz to estimate the average physical parameters of the diffuse HII region. The RMS electron density, emission measure, mass of the ionized gas and the number of Lyman continuum photons required to maintain ionization are listed in Table 3 (using Mezger and Henderson 1967). The exciting star types, assuming a single ionizing star are listed in the last column of Table 3 (Panagia 1973). G24.83+0.10 is the most massive HII region. In the next section, we discuss the observed recombination line emission from this region.

G24.74+0.08 : This diffuse region located due S of G24.83+0.10 (see Fig 2) does not have an associated IRAS point source. However, strong emission in the mid-infrared band E (MSX data) is observed, indicating its thermal nature and the predominance of hot dust. Moreover, MIR band A (MSX data), dominated by emission from polycylic aromatic hydrocarbons (PAH), is also detected from this region. The physical properties of this HII region estimated from its continuum strength are listed in Table 3.

G24.71-0.13 : This is another shell-like HII region. The size of the shell is about 7 pc similar to that of G24.83+0.10. G24.71-0.13 (see Fig 2) has a radio continuum peak in the middle of the two arcs forming the shell with diffuse emission along the rest of the shell. The IRAS point source IRAS 18340-0724 of strength 1322 Jy at 60μm is located close to the radio peak and is associated with the HII region. The properties of G24.71-0.13 derived from the continuum observations are listed in Table 3.

Other continuum sources : The HII regions G24.74+0.16, G24.74-0.2 and G24.68-0.16 are relatively compact with an angular extent less than $\sim$ 2'. All three

Table 4. Gaussian fits to the source-integrated line emission from the sources in the G24 region. The 1σ errors on the fitted parameters are given.

Source	Line	S_{int} mJy	V_{LSR} kms^{-1}	FWHM kms^{-1}	Reference
G24.83+0.10	H166α	153 ± 15	109 ± 4	20 ± 8	A
	H172α	179 ± 13	104.5 ± 1	30 ± 1.5	A
	H220α	250 ± 39	107 ± 1.5	19 ± 2	A
	H87α[1]	370	108.6 ± 0.4	26.9 ± 0.8	B
	H110α[2]	164	107	23	C
	H272α[3]	235	83 ± 2	77 ± 4	D
	C272α[3]		46 ± 2	34 ± 5	D

[1] integrated over $3'$; [2] integrated over $2.6'$;
[3] integrated over $2^\circ \times 6'$.
A. Present work; B. Lockman (1989)
C. Downes et al. (1980) ; D. Anantharamaiah (1985)

have associated IRAS point sources. G24.68-0.16 is the brightest among these four sources (2.3 Jy at 1.42 GHz). IRAS 18341-0727 with a flux density of 1322 Jy at 60μm associated with it. The emission is consistent with a free-free spectrum. This source appears to have a shell-like morphology with the shell opening to the E. G24.74+0.16 located to the W of G24.83+0.10 is the weakest continuum source in the field. The IRAS point source IRAS 18331-0715 of strength 326 Jy at 60μm is associated with this HII region. The derived physical properties of these HII regions are also listed in Table 3. An unresolved HII region, G24.92+0.08 (see Fig 1a) is located to the NE of G24.83+0.10. This HII region has an associated IRAS point source IRAS 18337-0707 with a strength of 256 Jy at 60μm.

4. The Recombination Line emission

Hydrogen RRLs from G24.83+0.10 were detected at all three observed frequencies. Fig 3 shows the spectra integrated over the diffuse emission at frequencies 1.42 ($n = 166$), 1.28 ($n = 172$) and 0.61 ($n = 220$) GHz. The feature detected at ~ 100 kms^{-1} is the hydrogen line. Gaussians were fitted to the hydrogen features at the observed frequencies and the results are shown in Table 4. We did not detect carbon RRL from G24.83+0.10 at any of the observed frequencies. If the carbon lines were formed in an associated PDR with $T_e \leq 400$ K, $n_e > 3$ cm^{-3} and pathlengths ≥ 11 pc, we should have been able to detect these near 1 GHz, with the sensitivity of our present observations.

The integrated line intensity map of the H166α emission (in grey) is shown in Fig 4 along with the radio continuum (in contours) at 1.42 GHz. Line emission

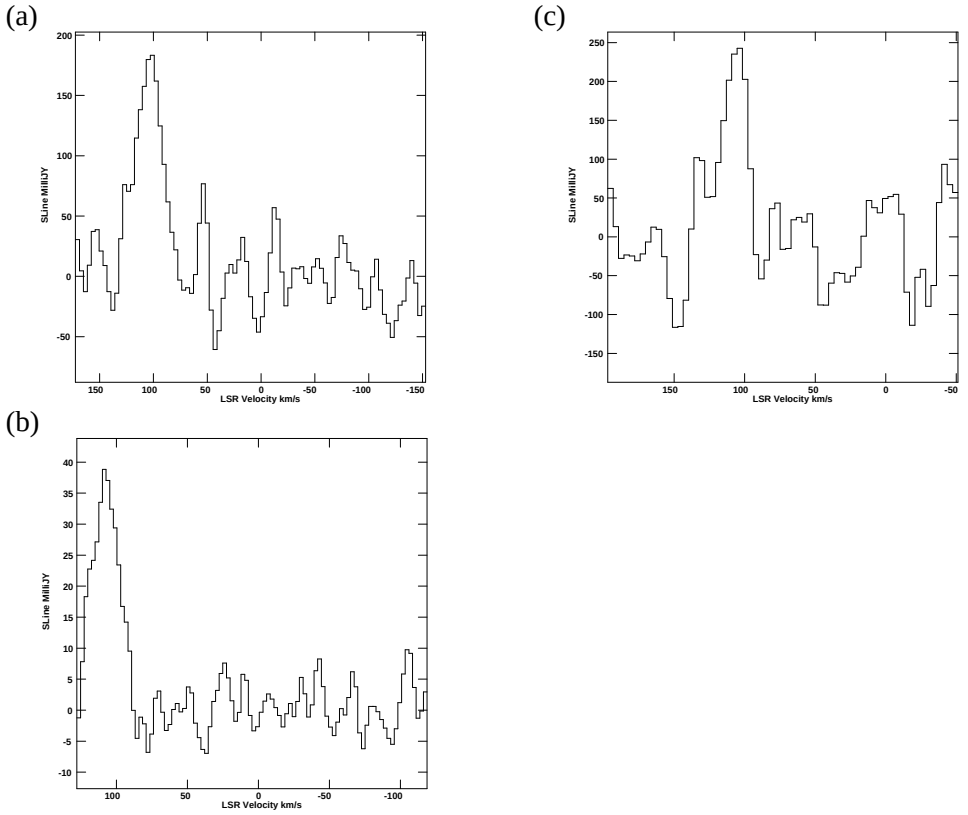

Figure 3. (a) The GMRT 172α spectrum integrated over G24.83+0.10. The spectrum has been Hanning smoothed to a velocity resolution of 7.2 kms^{-1}. **(b)** The GMRT 220α spectrum integrated over the continuum source G24.83+0.10. The spectrum has been Hanning smoothed to a velocity resolution of 7.6 kms^{-1}. **(c)** The VLA 166α spectrum integrated over a small region in G24.83+0.10 near G24.80+0.10 located in the W arc. The spectrum has been Hanning smoothed to a spectral resolution of 5.2 kms^{-1}. The feature near 100 kms^{-1} in all the three figures are the H RRLs.

from G24.83+0.10 follows the continuum morphology. Strongest line emission is observed near the compact objects G24.80+0.10 and and G24.85+0.09. Line emission is also observed from the diffuse source (see Fig 4). The line emission arising in G24.83+0.10 is observed at velocities ranging from ~ 100 to 110 kms^{-1}. No systematic gradient in the velocity is observed. Higher velocities $\sim 115 - 125$ kms^{-1} are observed for the RRL arising near the UCHII G24.80+0.09. From their high resolution CO observations, Furuya et al. (2002) find that the LSR velocity of the molecular cloud is about 111 kms^{-1} with velocity in the outflow ranging from 90 to 130 kms^{-1}. Thus, the RRL we detect near this UCHII region is likely related to this star forming region. Interestingly, the lines appear to be narrow with widths at half maximum of $12 - 24$ kms^{-1}. The narrow lines seem to arise close to the HII

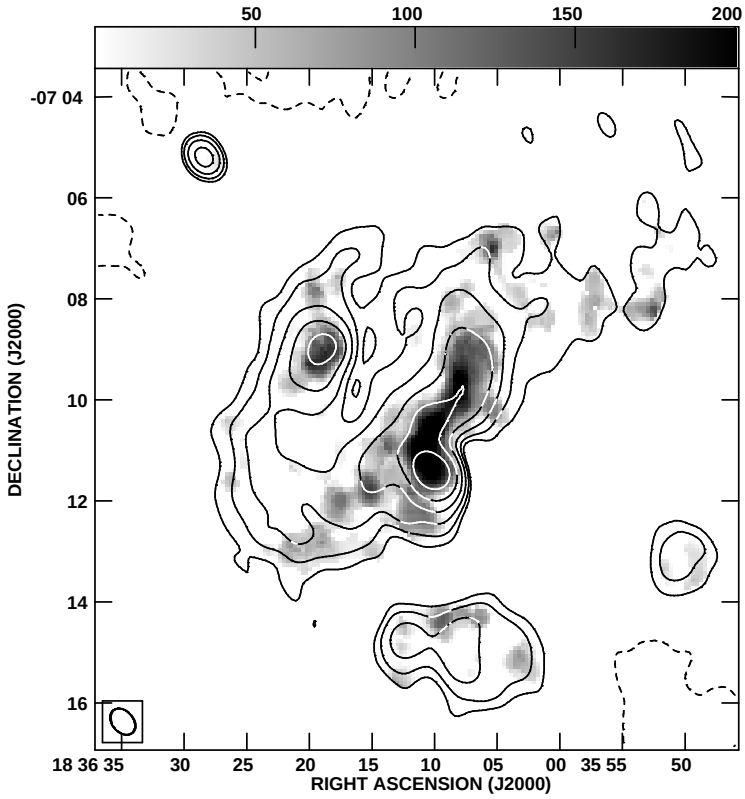

Figure 4. VLA Moment 0 image of H166α (grey scale) of the HII region G24.83+0.10 superposed on a contour map of the continuum emission from the region at 1.42 GHz. The image has a resolution of $35'' \times 25''$ PA$= 40^{\circ}$.

region G24.80+0.10 whereas the widest lines are observed near the UC HII region G24.85+0.09.

Weak H RRL emission from diffuse HII regions G24.74+0.08 and G24.74+0.16 is also detected (see Fig 4) at 102 kms^{-1} and 106 kms^{-1} respectively.

Due to the low signal-to-noise ratio for the H220α and H172α data, we were unable to obtain a detailed distribution of emission across G24.80+0.01. Thus, the integrated line flux densities of G24.83+0.10 at the three observed frequencies were used to model the line emission. The departure coefficients required in the models were calculated using the computer code of Salem & Brocklehurst (1979) , modified by Walmsley & Watson (1982) and Payne, Anantharamaiah and Erickson (1994) . These were then used to calculate the expected line flux density at the different quantum numbers following Shaver (1975) .

The best fitting model that we found had the following parameters, typical of a diffuse HII region: $T_e = 7000$ K and $n_e = 100$ cm^{-3} and a line of sight extent of 11 pc. The background radiation field for all the models was assumed to be a HII

region with an emission measure of 5×10^4 pc cm^{-6}. However we note that this model overpredicts the line flux near 0.61 GHz.

Detailed modelling of the observed RRLs should include contribution from both the diffuse HII region and the compact HII regions observed embedded within the diffuse shell. With the signal to noise of the current data, such a detailed model is not warranted. High resolution sensitive low frequency RRL observations are required to model different regions of G24.80+0.10 independently.

5. Summary

Using the GMRT and VLA, we have carried out low frequency interferometric continuum and recombination line observations of the HII regions near $l = 24^\circ.8$, $b = 0^\circ.1$ at 0.61 GHz, 1.28 GHz and 1.42 GHz. We detect continuum emission from ultra-compact, compact and extended HII regions. In this paper, we discuss the morphology and average properties of the HII regions using our continuum observations. G24.83+0.10, the main region under study in the paper, is diffuse and massive encompassing $\sim 550\ M_\odot$ within a linear size of 7 pc with a rms electron density of ~ 100 cm^{-3}. The source has a shell-like morphology with the shell opening to the N. Two IRAS point sources are clearly associated with this HII region. Compact HII regions are embedded in this diffuse region.

We detected H220α, H172α and H166α lines from G24.83+0.10. We also detected RRLs from two other HII regions in the field near 100 kms^{-1}. The model which provides the best fit to the source-integrated RRL data towards G24.83+0.1 has the following parameters: $T_e = 7000$ K, $n_e \sim 100$ cm^{-3} and path length of 11 pc. However this model overestimates the line strength at 0.61 GHz. We note that the electron density of the diffuse HII region that best fits the observed line data is similar to the rms electron density found from the continuum observations. More sensitive RRL observations of G24.83+0.10 are required to develop a detailed model of emission for this HII region.

Acknowledgments: We thank the anonymous referee for several useful comments which have especially helped improve the IR part of the paper. We thank the staff of the GMRT that made these observations possible. GMRT is run by the National Centre for Radio Astrophysics of the Tata Institute of Fundamental Research. The National Radio Astronomy Observatory is a facility of the National Science Foundation operated under cooperative agreement by Associated Universities, Inc. NGK thanks Prasad Subramanian for useful comments on the manuscript. The IRAS point source catalog was obtained from VizieR.

References

Ananthakrishnan, S. & Rao, A. P., 2002, In Manchanda, R. K., & Paul, B., editors, *Multi-colour Universe*

Anantharamaiah, K. R., 1985, *J Astrophys. Astron.*, **6**, 177.
Codella, C., Felli, M., Natale, V., 1994, *Astron. & Astrophy.*, **284**, 233.
Conti, P. & Crowther, P. A., 2004, *Mon. Not. R. Astron. Soc.*, **355**, 899.
Downes, D., Wilson, T. L., Bieging, J., Wink, J., 1980, *Astron. & Astrophy. Supple.* , **40**, 379.
Dravskikh, Z. V., & Dravskikh, A. F., 1964, *Astron. Tsirk*, **158**, 2.
Furuya, R. S., Cesaroni, R., Codella, C., et al., 2002, *Astron. & Astrophy.*, **390**, L1.
Haslam, C. G. T., Salter, C. J., Stoffel, H., Wilson, W. E., 1982, *Astron. & Astrophy. Supple*, **47**, 1.
Heiles, C., Reach, W. T., & Koo, B-C., 1996, Astrophy. J., **466**, 191.
Lockman, F. J., 1989, Astrophy. J., **71**, 469.
Lockman, F. J., Pisano, D. J., Howard G. J., 1996, *Astrophy. J.*, **472**, 173.
Mezger, P. G., & Henderson, A. P., 1967, *Astrophy. J.*, **147**, 471.
Palmer, P., Zuckermann, B., Penfield, H., Lilley, A. F., Mezger, P. G., 1967, *Astron. J.*, **72**, 821.
Panagia, N., 1973, Astron. J., **78**, 929.
Payne, H. E., Anantharamaiah, K. R., Erickson, W. C., 1994, Astrophy. J., **430**, 690.
Roshi, D. A. & Anantharamaiah, K. R., 2001, Astrophy. J., **557**, 226.
Salem, M. & Brocklehurst, M., 1979, *Astrophy. J. Supple*, **39**, 633.
Shaver, P. A. 1975, *Pramana*, **5**, 1.
Sorochenko, R. L. & Borozich, E. V. 1964, *Rep. of Sov. Acad. of Sci.*, **162**, 603.
Swarup, G., Ananthakrishnan, S., Kapahi, V. K., et al. 1991, *Current Science*, **60**, 95.
Walmsley, C. M., & Watson, W. D., 1982, Astrophy. J., **260**, 317.